The formation of shear-band/fracture networks from a constitutive instability: Theory and numerical experiment

A.I. Chemenda

The formation of shear-band/fracture networks from a constitutive instability: Theory and numerical experiment

A. I. Chemenda[1]

Received 2 March 2007; revised 15 August 2007; accepted 29 August 2007; published 27 November 2007.

[1] A mono-shear-band bifurcation analysis is extended to the formation of shear-band network affecting a finite brittle body. This analysis, along with the results of numerical simulations, suggests the following description of the bifurcation process. It starts when the hardening modulus h reaches a critical value h_{max} which has proved to be the same as that previously obtained from mono-band analysis. The deformation pattern is penetrative at this stage and presents two conjugated sets of dense, parallel intermittent bands with accelerated and decelerated inelastic deformation. At the next stage the response of the material outside the bands with accelerated deformation becomes elastic (elastic unloading). The size of the elastic zones rapidly grows and the spacing λ between the "active" localization bands (incipient fractures) correspondingly increases to a value defined by the constitutive and stress-state parameters. Both the analytical solution and numerical models show that λ is very sensitive to h: $\lambda = \infty$ at $h = h_{max}$ and λ tends to the bend thickness when $h \rightarrow h_{min} < h_{max}$. If h reduces rapidly below h_{min}, the deformation "jumps" into the post-localization state and the material becomes completely crushed. Thus there exists only a narrow range of h values for which the deformation bifurcation, and hence the formation of regular band/fracture network, is possible. The obtained analytical solutions show how the band spacing depends on other constitutive parameters and on the stress-state.

Citation: Chemenda, A. I. (2007), The formation of shear-band/fracture networks from a constitutive instability: Theory and numerical experiment, *J. Geophys. Res.*, *112*, B11404, doi:10.1029/2007JB005026.

1. Introduction

[2] There are numerous laboratory (Figures 1a and 1c) and field (Figures 1d and 1e) examples of a surprisingly regular organization of fracture/band patterns in different materials. This kind of organization was also reproduced numerically [e.g., *Poliakov et al.*, 1994]. The likely mechanism for the formation of such regular sets of parallel fractures is the bulk loss of stability of the material. The physical nature of this instability can lie in the nonlinearity of the material properties and their change (e.g., degradation) during inelastic deformation. Such a material can undergo uniform straining only until a certain degree of its damage, after which the deformation cannot be homogeneous anymore and localizes in certain zones, such as planar bands. The prediction of the conditions for localization and of the characteristics of the resulting macro-fractures (e.g., their spatial organization) can be based on the complete micromechanical description, which considers the formation and interaction of micro-cracks, grain rotations, pore collapse, etc. There is, however, a simpler and more elegant way to approach this problem by assuming the concept of deformation bifurcation within the frame of macroscopic "smooth" description of constitutive properties [*Rice*, 1973]. The bifurcation results from a constitutive (internal or material) instability associated with instabilities in mathematical solutions to incremental deformation boundary-value problems.

[3] The bifurcation theory has been developed by *Hadamard* [1903], *Thomas* [1961], *Hill* [1962], and *Mandel* [1964, 1966]. They obtained the bifurcation condition as a particular case of "stationary discontinuity (or acceleration/plastic wave)" corresponding to slip surfaces, Luders lines or localization bands. The condition relates the orientation of a band with elasto-plastic stiffness moduli (4th order stiffness tensor) that depend on the constitutive formulation. *Rudnicki and Rice* [1975] (hereafter RR) tied the bifurcation theory to the realistic constitutive model for geomaterials. From the bifurcation condition they derived both the orientation of a shear band in the stress space (Figure 2) and the critical hardening modulus (at which strain localization should start) as functions of the constitutive and stress-state parameters. This paper gave rise to the numerous studies of deformation localization (see *Vardoulakis and Sulem* [1995] and *Bésuelle and Rudnicki* [2004] for a review).

[4] The above shear-band bifurcation theory deals in fact with formation (initiation) of one infinitely long localization band within an infinite body. In reality, however, instead of one band we observe the formation of band (fracture) networks (Figure 1) within a finite (frequently layered) body. The band/fracture networks are clearly characterized by certain dominant (for each case) spacing. This parameter

[1]Géosciences Azur, Université de Nice-Sophia Antipolis and CNRS, Valbonne, France.

0148-0227/07/2007JB005026$09.00

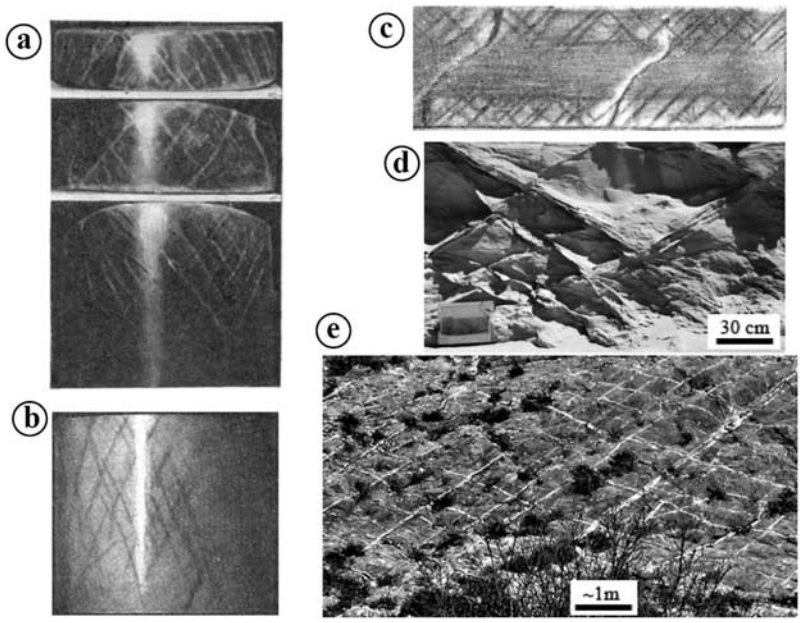

Figure 1. Shear-band (fracture) networks in laboratory samples (a to c) and field (d and e). (a) Paraffin and (b) marble cylinder samples deformed under axi-symmetric compression; (c) iron bar submitted to a flexure; (d) Upper-Cretaceous sand, north-east of Carpentras, Southern France (courtesy of Ch. Wibberley; geological details are in [*Wibberley et al.*, 2007]); (e) Upper-Cretaceous sandstone, Orange, Provence (France) (courtesy of E. Saillet). Samples in Figures 1a to 1c (photos are from Nadai [1950]) have centimetric size (the exact dimensions are not indicated).

is extremely important for the reservoir applications dealing with reservoir permeability (fracture/double porosity, hydraulic barriers, etc.). The definition of band spacing is obviously beyond the limits of mono-band analysis. Garagash [*Garagash*, 1981; *Garagash and Nikolaevsky*, 1989] extended such analysis onto a parallel set of infinitely long shear bands based on the virtual work principle. He obtained the RR's critical condition for hardening modulus as a limit case corresponding to the infinite spacing between the bands in the regime of elastic unloading outside them.

[5] The next step in approaching the real conditions should be an analysis of the formation of two parallel conjugated band sets (as seen in Figure 1) within a finite body. Such an analysis is attempted in the present paper. The same approach is used as in the classical bifurcation theory. The difference consists in the velocity field during the loss of the constitutive stability which has been designed to correspond to a regular band network in Figure 3a. The form of this field is derived from the experimentally inspired assumption that during bifurcation the deformation pattern represents a spatially repeating structure which can be composed of one elementally sell (Figure 3) whose size defines the dominant band spacing. The analysis is then limited to this cell. The velocity field within it is obtained from another assumption, that at the moment of bifurcation the deformation within the cell is completely due to the internal energy redistribution with no external energy input to the cell. The obtained bifurcation equation, containing the spacing parameter, has been analyzed for two cases corresponding respectively to the continuous and discontinuous bifurcation (with inter-band unloading in the latter case). For the first case we obtained the same as RR's critical conditions for the hardening modulus and the band orientation, with the spacing parameter being canceled out. In the second case this parameter has been found as a function of all constitutive parameters including the hardening modulus. These analytical results have been tested on and supported by the final-difference numerical models.

2. Summary of the Mono-Shear-Band Bifurcation Theory

[6] The general concept of bifurcation from homogeneous deformation as a result of instability in the constitutive description has been developed by *Hadamard* [1903],

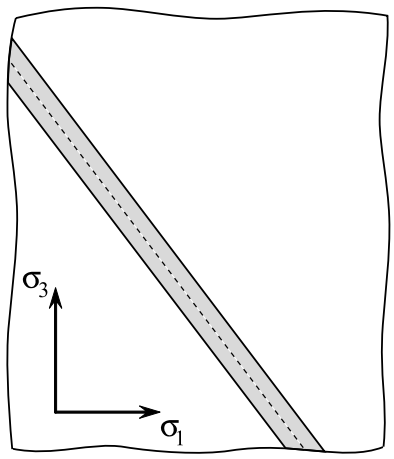

Figure 2. Localization band in an infinite body: mono-shear-band localization model. σ_i are the principal stresses.

Thomas [1961], *Hill* [1962], and *Mandel* [1964, 1966]. The constitutive instability is viewed as a formation of a narrow planer band of deformation localization within an infinite body at a certain stage of its initially uniform deformation under uniform stressing [*Berg*, 1970, *Rice*, 1973]. Outside the band the velocity field remains uniform and within it varies only in the direction normal to the band. The difference between the deformation rate outside the band, $D_{ij}^{(2)}$, and inside it, $D_{ij}^{(1)}$, can be presented

$$D_{ij} = D_{ij}^{(1)} - D_{ij}^{(2)} = \frac{1}{2}\left[n_j g_i(\mathbf{n}\cdot\mathbf{x}) + n_i g_j(\mathbf{n}\cdot\mathbf{x})\right] \quad (1)$$

where g_i are non-zero only within the band (D_{ij} has vanishing intermediate principal value), x_i are the principal axes, and $\mathbf{n}$ (n_i) is the unit normal to the band (i = 1, 2, 3). The condition of the continuity of the traction rate at the band interfaces can be written

$$n_i\dot{\sigma}_{ij} = n_i\left(\dot{\sigma}_{ij}^{(1)} - \dot{\sigma}_{ij}^{(2)}\right) = 0 \quad (2)$$

where $\dot{\sigma}_{ij}^{(r)}$ (r = 1, 2) are the material time derivatives of true (Cauchy) stress at the internal (r = 1) and external (r = 2) sides of the band, respectively. The strain and deformation rates are related by a linear, homogeneous tensor relation

$$\dot{\sigma}_{ij}^{(r)} = L_{ijkl}^{(r)} D_{kl}^{(r)}. \quad (3)$$

[7] For the case when the incremental elasto-plastic stiffness tensor L_{ijkl} is the same within and outside the band (3) becomes

$$\dot{\sigma}_{ij} = L_{ijkl} D_{kl}. \quad (4)$$

[8] Combining (1), (2), and (4) yields a set of linear, homogeneous in g's equations

$$\left(n_i L_{ijkl} n_l\right) g_k = 0,$$

which have nontrivial solution when

$$\det\left|n_i L_{ijkl} n_l\right| = 0. \quad (5)$$

[9] This characteristic equation represents the condition for the deformation bifurcation when a non-uniform (with $g_i \neq 0$) continuation of deformation is possible. The bifurcation condition relates the orientation (n_i) of the band with moduli L_{ijkl}. *Hill* [1962] obtained this condition by using in (2) the intrinsic derivative of the first Piola-Kirchhoff stress $\dot{\pi}_{ij}$ and in (4) the convected derivative of the contravariant Kirchhoff stress $\dot{\alpha}_{ij}$ instead of $\dot{\sigma}_{ij}$. Replacement of $\dot{\pi}_{ij}$ and $\dot{\alpha}_{ij}$ by $\dot{\sigma}_{ij}$ in (2) and (4) means that we neglect the rotational effects and consider that the acting stresses are small compared to the stiffness moduli (although for the field (1) equation (2) is simply equivalent to $n_i\dot{\pi}_{ij} = 0$ [RR; *Rice*, 1976]).

[10] To complete the bifurcation analysis and to find the critical relations between the orientation n_i of the band plan, the constitutive parameters and the stress-state, one has to specify the modulus tensor L_{ijkl} which depends on the choice of constitutive model.

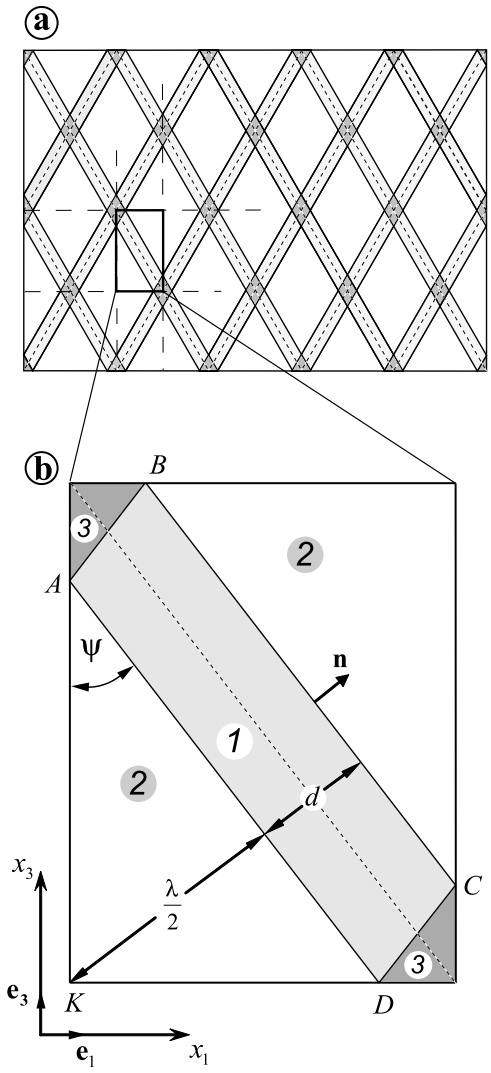

Figure 3. Regular shear-band network. (a) Localization pattern composed of two conjugated sets of parallel shear bands; (b) elementary cell. d is the shear band thickness and λ is the inter-band distance. 1, 2, and 3 denote zones with different deformation fields. $\mathbf{e_i}$ are the unit vectors.

2.1. Constitutive Equations

[11] Consider simple isotropic-hardening model with smooth both yield $f(\sigma_{ij})$ and plastic potential $\Phi(\sigma_{ij})$ functions. Assume two-invariant Drucker-Prager functions

$$f = \bar{\tau} + \alpha\sigma - k \quad (6)$$

$$\Phi = \bar{\tau} + \beta\sigma \quad (7)$$

where α is the internal friction coefficient; k is the internal cohesion; β is the dilation factor; $\bar{\tau} = \left(\frac{1}{2}s_{ij}s_{ij}\right)^{1/2}$ is the intensity of shear stress approximately equal to the maximal shear stress; $s_{ij} = \sigma_{ij} - \delta_{ij}\sigma$ is the stress deviator, δ_{ij} is the Kronecker delta, and $\sigma = \frac{1}{3}\sigma_{ii}$ is the mean stress (i, j = 1, 2, 3).

The total incremental strain represents the sum of increments of elastic and inelastic strains:

$$d\varepsilon_{ij} = d\varepsilon^e_{ij} + d\varepsilon^p_{ij}, \tag{8}$$

where elastic strains are related to stresses by Hook's equations:

$$d\varepsilon^e_{ij} = \frac{d\sigma}{K}\delta_{ij} + \frac{ds_{ij}}{2G}. \tag{9}$$

[12] The inelastic strain increments follow from the plastic potential function

$$d\varepsilon^p_{ij} = d\lambda\frac{\partial\Phi}{\partial\sigma_{ij}} = d\lambda\left[\frac{s_{ij}}{2\bar{\tau}} + \frac{1}{3}\beta\delta_{ij}\right]. \tag{10}$$

[13] Here K and G are the bulk and shear modulus, respectively, and $d\lambda$ is non-negative scalar function to be found. For the relative incremental inelastic volume change, equations (10) yield

$$d\varepsilon^p = d\varepsilon^p_{ii} = \beta d\lambda. \tag{11}$$

[14] The dilation relation between the inelastic volumetric and shear deformation [*Reynolds*, 1885] can be presented in the following form [*Nikolaevskiy*, 1967]

$$d\varepsilon^p = \beta d\bar{\gamma}^p \tag{12}$$

where $d\bar{\gamma}^p = (2de^p_{ij}\, de^p_{ij})^{1/2}$ and $de^p_{ij} = d\varepsilon^p_{ij} - \frac{1}{3}\delta_{ij}\, d\varepsilon^p_{kk}$. Using (11) and (12) in (10) results in

$$d\varepsilon^p_{ij} = d\bar{\gamma}^p\left[\frac{s_{ij}}{2\bar{\tau}} + \frac{1}{3}\beta\delta_{ij}\right]. \tag{13}$$

[15] The closing relation follows from the Prager consistency equation for the yield function

$$df = \frac{\partial f}{\partial\sigma_{ij}}d\sigma_{ij} + \frac{\partial f}{\partial\bar{\gamma}^p}d\bar{\gamma}^p = 0. \tag{14}$$

[16] Considering that the properties change during inelastic deformation and that the material can either harden or weaken, assume that α and k are functions of $\bar{\gamma}^p$: $\alpha\,(\bar{\gamma}^p)$ and $k(\bar{\gamma}^p)$, where $\bar{\gamma}^p = \int(2de^p_{ij}\, de^p_{ij})^{1/2}$. It follows then from (14) that

$$d\bar{\tau} + \alpha d\sigma - Hd\bar{\gamma}^p = 0, \tag{15}$$

where $H = \frac{dk}{d\bar{\gamma}^p} - \sigma\frac{d\alpha}{d\bar{\gamma}^p}$ is the plastic hardening modulus.

[17] Combining (8), (9), (13), and (15) relate directly the incremental stress $d\sigma_{ij}$ and incremental strain $d\varepsilon_{ij}$ (or the stress and deformation rates) and obtain for the stiffness tensor [RR]

$$L_{ijkl} = G\left\{\left[\left(\delta_{ik}\delta_{jl} + \delta_{il}\delta_{kj}\right) + \left(\frac{K}{G} - \frac{2}{3}\right)\delta_{kl}\delta_{ij}\right] - \frac{G}{(H+G) + \alpha\beta K}\left(N_{ij} + \frac{K}{G}\beta\delta_{ij}\right)\left(N_{kl} + \frac{K}{G}\alpha\delta_{kl}\right)\right\} \tag{16},$$

where $N_{ij} = \frac{s_{ij}}{\bar{\tau}}$.

2.2. Critical Hardening Modulus and Orientation of a Shear Band

[18] Submitting (16) into (5) and solving the resulting equation for H, RR found

$$H = 3\frac{\left(Gn_iN_{ij}n_j + \beta K\right)\left(Gn_kN_{kl}n_l + \alpha K\right)}{(4G + 3K)} + G\left[\left(n_iN_{ij}n_kN_{kj}\right) - \left(n_iN_{ij}n_j\right)^2\right] - (G + \alpha\beta K). \tag{17}$$

[19] They searched out the plane corresponding to the maximal H over all orientations n_i. This plan was proven to be parallel to the intermediate principal direction σ_2 and inclined to σ_3 direction under angle ψ defined as

$$tg^2\psi = -\frac{2(1+\nu)(\alpha+\beta) - 3\left[(1-2\nu)N + \sqrt{4-3N^2}\right]}{2(1+\nu)(\alpha+\beta) - 3\left[(1-2\nu)N - \sqrt{4-3N^2}\right]}, \tag{18}$$

where $N = \frac{s_2}{\bar{\tau}}$ is the stress-state parameter, s_2 is the intermediate principal deviatoric stress, and $\nu = \frac{3K-2G}{6K+2G}$ is the Poisson ratio. (The compressive stress is negative and $\sigma_3 < \sigma_2 < \sigma_1$). The critical hardening modulus follows from (17) and (18)

$$h_{cr} = \frac{H_{cr}}{G} = \frac{1+\nu}{9(1-\nu)}(\beta-\alpha)^2 - \frac{1+\nu}{2}\left(N + \frac{\alpha+\beta}{3}\right)^2. \tag{19}$$

Conditions (18) and (19) are valid for [*Perrin and Leblond*, 1993] (see also [*Issen and Rudnicki*, 2000]),

$$N(1-2\nu) - \sqrt{4-3N^2} \le \frac{2}{3}(\nu+1)(\alpha+\beta) \le N(1-2\nu) + \sqrt{4-3N^2}. \tag{20}$$

[20] RR also obtained corrections of ψ and h_{cr} for the co-rotational terms in the stress derivative by replacing in (2) and (4) the material time derivative by the invariant to rigid body spins Jaumann derivative $\overset{\nabla}{\sigma}_{ij}$ of the Cauchy stress ($\overset{\nabla}{\sigma}_{ij} = \dot{\sigma}_{ij} - W_{ik}\,\sigma_{kj} + \sigma_{ik}\,W_{kj}$, where $W_{ij} = \frac{1}{2}(\upsilon_{i,j} - \upsilon_{j,i})$, and υ_i is the velocity field in the Eulerian coordinates, the subscript comma denoting spatial differentiation. The obtained corrections for both parameters are on the order of $\bar{\tau}/G$ and can be essential when the predicted by (19) H_{cr} is as small as to be comparable to the maximal shear stress (see also [*Rice*, 1976]).

3. Formation of Shear-Band Network

[21] Consider now the condition for bifurcation of the homogeneous deformation field into the regular deformation pattern in Figure 3. This pattern is formed under initially uniform stressing by two conjugated families of parallel shear bands. The pattern is symmetric with respect to two principal directions x_1 and x_3, and parallel to x_2. The band network is characterized by the existence of an elementary cell (Figure 3) of which the whole pattern can be composed. It is sufficient thus to obtain the bifurcation condition for this cell.

3.1. Deformation Rate Field Within the Elementary Cell at the Onset of Bifurcation

[22] Assume that the onset of bifurcation occurs at fixed boundaries of the body (without external energy supply). In this case the boundaries of an elementary cell can be considered as fixed as well. Divide the elementary cell into three zones with different velocity fields (Figure 3b). On the basis of the symmetry of the problem consider that in all zones the deformation is uniform and in zone (2) the material undergoes only stretching/shortening in two principal directions x_1 and x_3

$$D_{kl}^{(2)} = B_k \delta_{kl} \quad k,l = 1,3 \tag{21}$$

[23] The velocity vectors in points A, C, D, and B in Figure 3b are, respectively

$$\boldsymbol{v}_A = -\boldsymbol{v}_C = \frac{\lambda B_3}{2n_3}\mathbf{e}_3;\ \boldsymbol{v}_D = -\boldsymbol{v}_B = \frac{\lambda B_1}{2n_1}\mathbf{e}_1 \tag{22}$$

[24] Using (22) and assuming that the deformation in zone (1) is uniform, one obtains for the deformation rate in this zone

$$D_{kl}^{(1)} = C_{klm}B_m, \tag{23}$$

where

$$C_{111} = \frac{n_3^2(5\chi-1)-\chi-1}{2\chi};\ C_{113} = \frac{n_1^2(1-\chi)}{2\chi};$$
$$C_{131} = \frac{n_3^2(3\chi-1)-2\chi}{2\chi n_1 n_3^{-1}};\ C_{133} = \frac{n_3^2(1-3\chi)+\chi-1}{2\chi n_3 n_1^{-1}}$$
$$C_{311} = \frac{n_3^2(3\chi-1)-2\chi}{2\chi n_1 n_3^{-1}};\ C_{331} = \frac{n_3^2(1-\chi)}{2\chi};$$
$$C_{313} = \frac{n_3^2(1-3\chi)+\chi-1}{2\chi n_3 n_1^{-1}};\ C_{333} = \frac{n_3^2(1-5\chi)+4\chi-2}{2\chi},$$

k, l, m = 1, 3, $\chi = \frac{d}{\lambda}$ is the band spacing parameter, and

$$n_i \neq 0. \tag{24}$$

[25] For zone (3) it can be supposed $D_{kl}^{(3)} = -\frac{B_k}{\chi}\delta_{kl}$, but we do not need it for the following as the analysis can be limited to zones (1) and (2).

[26] Since the deformation field is uniform in these zones, the equilibrium equations are met in both and the stress can change only at the band boundary in the direction perpendicular to it. Therefore the equations of continuing equilibrium can be written

$$\dot{\sigma}_{ij,i} = \frac{\partial \dot{\sigma}_{ij}}{\partial(n_i x_i)}\frac{\partial(n_i x_i)}{\partial x_i} = \frac{\partial(n_i \dot{\sigma}_{ij})}{\partial(n_i x_i)} = 0.$$

[27] This leads to condition (2), which thus holds valid for our velocity field. Submitting (21) and (23) into (3) and the result into (2) yields

$$n_i\left(L_{ijkl}^{(1)}C_{klm} - L_{ijmp}^{(2)}\right)B_m = 0$$

(i, j, k, l, m = 1, 3, and $p = m$). The corresponding characteristic equation (bifurcation condition) is

$$\det\left|n_i\left(L_{ijkl}^{(1)}C_{klm} - L_{ijmp}^{(2)}\right)\right| = 0. \tag{25}$$

3.2. Continuous Bifurcation

[28] For this case $L_{ijkl}^{(1)} = L_{ijkl}^{(2)} = L_{ijkl}$ and equation (25) after submission of (16) and the expressions for C_{klm} from (23) becomes

$$2\left(3\zeta^2\chi^2 - \zeta^2\chi - \chi - 1\right)\left[\zeta^2 + \zeta Q\left(L_{ijkl}\right) + R\left(L_{ijkl}\right)\right] = 0 \tag{26}$$

where

$$\xi = n_3^2 - n_1^2 = \cos 2\psi \tag{27}$$

and the coefficients $Q(L_{ijkl})$ and $R(L_{ijkl})$ are

$$Q = \frac{2[3N(1-2\nu) - 2(\nu+1)(\alpha+\beta)]}{3\sqrt{4-3N^2}}$$
$$R = \frac{72(1-2\nu)h + 9N^2(5-4\nu) + 4(\nu+1)[8\alpha\beta + 3N(\alpha+\beta)]}{9(4-3N^2)} \tag{28}$$

[29] The problem is thus reduced to the analysis of a quadratic equation

$$\zeta^2 + Q\zeta + R = 0. \tag{29}$$

[30] The deformation bifurcation is possible when this equation has real roots, i.e., when

$$Q^2 - 4R \geq 0 \tag{30}$$

[31] Submitting (28) into this inequality yields

$$h = \frac{H}{G} \leq h_{cr} = \frac{1+\nu}{9(1-\nu)}(\beta-\alpha)^2 - \frac{1+\nu}{2}\left(N + \frac{\alpha+\beta}{3}\right)^2 \tag{31}$$

[32] The obtained maximal normalized hardening modulus h_{cr} corresponding to the onset of deformation localization during progressive loading of the material was proven thus to be the same as in (19). At $h = h_{cr}$ the left part of (30) vanishes and the solution of (29) defining the orientation of the localization bands becomes

$$\zeta = -\frac{Q}{2} = \frac{2(1+\nu)(\alpha+\beta+3N) - 9N}{3\sqrt{4-3N^2}}. \tag{32}$$

[33] This expression is equivalent to (18). According to (24) and (27) the critical condition (31) is valid for $-1 < \zeta < 1$, which yields the same condition as (20), but without equalities

$$N(1-2\nu) - \sqrt{4-3N^2} < \frac{2}{3}(\nu+1)(\alpha+\beta)$$
$$< N(1-2\nu) + \sqrt{4-3N^2}. \tag{33}$$

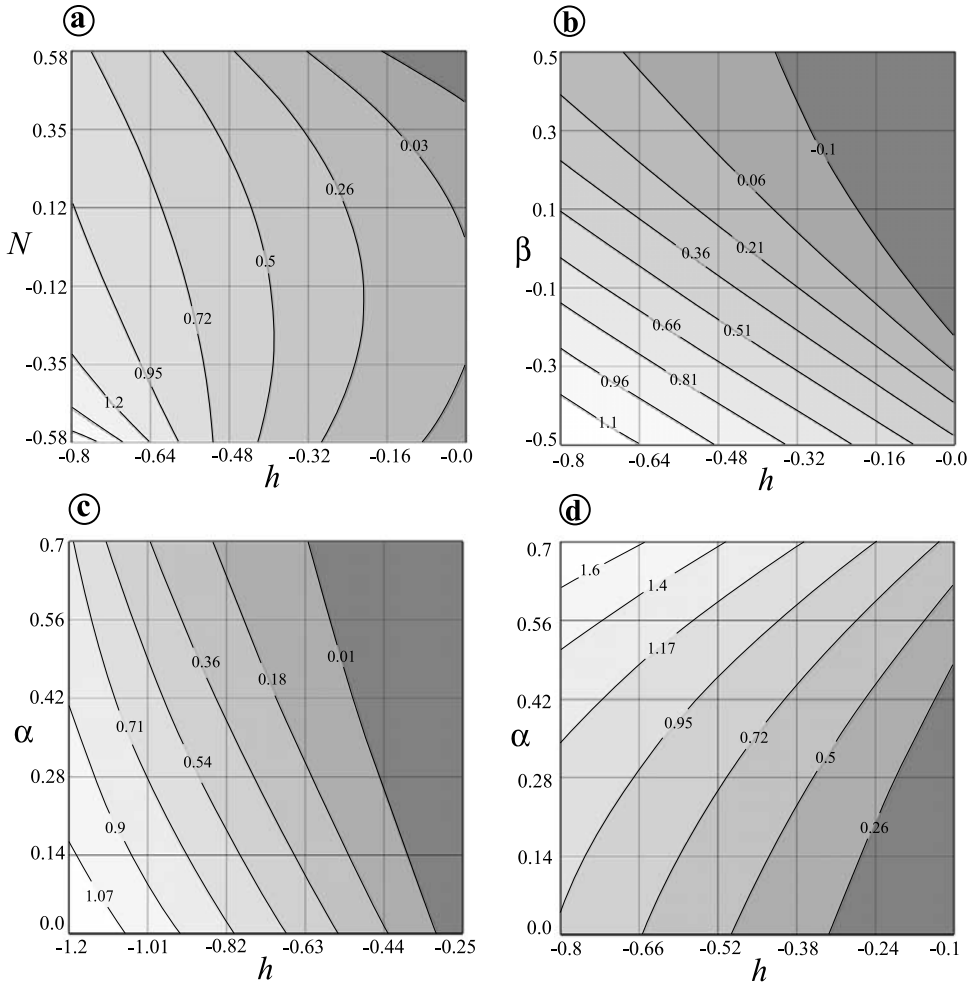

Figure 4. Contour plots of the obtained solution $\chi(\alpha, \beta, \nu, N, h)$: (a) $\chi(N, h)$ for $\alpha = 0.5$, $\beta = 0$, and $\nu = 0.3$; (b) $\chi(\beta, h)$ for $\alpha = 0.5$, $N = 0.577$, and $\nu = 0.3$; (c) $\chi(\alpha, h)$ for $\beta = -0.5$, N = 0.577, and $\nu = 0.3$; (d) $\chi(\alpha, h)$ for $\beta = 0.5$, $N = 0.577$, and $\nu = 0.3$.

[34] We thus obtained a quite surprising result: despite using the velocity field corresponding to two conjugated families of the localization bands within a finite body instead of field (1) corresponding to a single localization band within an infinite body, both the critical condition for the localization and the band orientation are the some in both cases.

[35] Although the band spacing parameter χ is present in equation (26) it does not enter the final equation (29) and therefore the expressions (31) and (32). The fact that the spacing is not defined could mean that the shear banding at the initial (first) stage of deformation bifurcation is penetrative and affects the whole body.

[36] The constitutive response is the same throughout the body at the onset of bifurcation. On the other hand, since the deformation occurs more rapidly within the localization bands than outside, the damage accumulation (property change) within the bands is also more rapid. If the boundaries of the elementary cell are fixed (the average deformation of the elementary cell is zero or small), the acceleration of the deformation (loading) along the localization bands will be associated with the deformation deceleration (unloading) outside the bands. Therefore at the next stage of bifurcation the constitutive response outside the bands will become elastic which corresponds to the discontinuous bifurcation. Note, that the possibility of the transition from the continuous to discontinuous bifurcation has been discussed by *Rice and Rudnicki* [1980] in the single-band context.

3.3. Elastic Unloading Outside Shear Bands

[37] In the following we assume that the orientation of the localization bands is acquired at first, continuous stage of bifurcation as defined by (32), and that the hardening modulus reduces rapidly (instantaneously) to some value $h \leq h_{cr}$. This corresponds to rather brittle material behavior with elastic unloading outside the localization bands. For this case $L^{(1)}_{ijkl} = L_{ijkl}$ from (16) and

$$L^{(2)}_{ijkl} = G\left\{\left[\left(\delta_{ik}\delta_{jl} + \delta_{il}\delta_{kj}\right) + \left(\frac{K}{G} - \frac{2}{3}\right)\delta_{kl}\delta_{ij}\right]\right. \qquad (34)$$

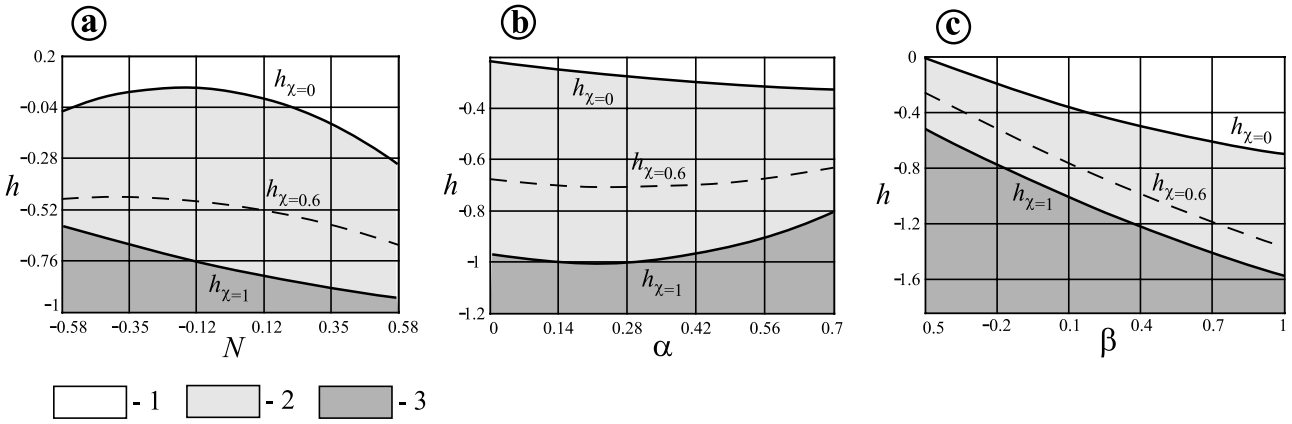

Figure 5. Plots of critical hardening moduli versus N, α, and β. 1, Range where no localization (macro-fracturing) is possible; 2, range where regular localization banding (macro-fracturing) is possible; 3, range corresponding to the complete crushing of the material. The curves also are shown for $\chi = 0.6$ the maximal χ value at which the deformation localization is "resolved" in the numerical models (see Figure 9). The curves for $h_{\chi=0}$ and $h_{\chi=1}$ are from (36) and (37), respectively. (a) $\alpha = 0.3$, $\beta = 0$, and $\nu = 0.3$; (b) $\beta = 0$, $N = 0.577$, and $\nu = 0.3$, and (c) $\alpha = 0.3$, $N = 0.577$, and $\nu = 0.3$.

(we consider here that the elastic properties do not change during deformation). Submitting these expressions for the stiffness tensors into (25) yields:

$$\det|A_{jm}| = 0 \tag{35}$$

where

$$A_{11} = -k_1 L^{(1)}_{1111} + k_2 L^{(1)}_{1133} + 2k_3 k_4 L^{(1)}_{1313} + k_8 L^{(2)}_{1111},$$

$$A_{13} = k_5 L^{(1)}_{1111} + k_6 L^{(1)}_{1133} + 2k_7 L^{(1)}_{1313} + k_8 L^{(2)}_{1133},$$

$$A_{31} = -2k_4 L^{(1)}_{1313} - k_1 L^{(1)}_{3311} + k_2 L^{(1)}_{3333} + k_8 L^{(2)}_{3311},$$

$$A_{33} = -2k_3^{-1} k_7 L^{(1)}_{1313} + k_5 L^{(1)}_{3311} + k_6 L^{(1)}_{3333} + k_8 L^{(2)}_{3333};$$

$$k_1 = \zeta(5\chi - 1) - 3(\chi - 1);\ k_2 = (\zeta - 1)(\chi - 1);$$
$$k_3 = \frac{\zeta - 1}{\zeta + 1}; k_4 = \zeta(3\chi - 1) + \chi + 1; k_5 = (\zeta + 1)(1 - \chi);$$
$$k_6 = \zeta(5\chi - 1) + 3(\chi - 1);\ k_7 = \zeta(3\chi - 1) - \chi - 1;\ k_8 = -4\chi$$

and ζ is given by (32). Equation (35) has been solved analytically for $\chi(\alpha, \beta, \nu, N, h)$ and $h(\alpha, \beta, \nu, N, \chi)$ using Mathcad software. The obtained solutions are valid for the range (33). They are very cumbersome (occupy several pages each), therefore we present them only graphically (Figures 4 and 5). The structure of the solution for h is $h = h_{cr} + \chi\wp(\chi, \alpha, \beta, \nu, N)$. It has compact explicit form only for $\chi = 0$ and $\chi = 1$:

$$h_{\chi=0} = h_{cr} = \frac{1+\nu}{9(1-\nu)}(\beta - \alpha)^2 - \frac{1+\nu}{2}\left(N + \frac{\alpha + \beta}{3}\right) \tag{36}$$

$$h_{\chi=1} = h_{cr} + \frac{(\nu+1)(\beta-\alpha)}{3(1-\nu)}\left[\frac{N}{4} + \frac{\alpha(\nu+1)}{3(2\nu-1)}\right] + \frac{3}{4}N^2 - 1 \tag{37}$$

[38] For $h = h_{\chi=0}$ the solution $\chi(\alpha, \beta, \nu, N, h)$ yields $\chi = 0$. It follows that when the elastic unloading occurs at $h = h_{\chi=0}$, the distance between the localization bands is infinite meaning that under this condition only one band (fracture) will be initiated within an infinite body. With the reduction of h (at other parameters constant) the distance between the bands/fractures reduces (spacing parameter χ increases). The band/fracture pattern reaches "saturation" at $h = h_{\chi=1}$ when the band thickness is equal to the inter-band distance. At $\chi > 1$ the material is completely crushed and regular fracture pattern formed previously (if any) should be "erased". There exists thus a limited band for the h values, $h_{\min} = h_{\chi=1} \le h \le h_{\chi=0} = h_{\max}$, for which the formation of the regular fracture pattern is possible (Figure 5).

4. Numerical Test

[39] The best way to check the validity of the obtained results is to test them against experimental data, but the appropriate data are not available. Therefore we proceeded to numerical test. Accurate numerical simulation of constitutive instability (as of any other spontaneous physical instability) is a delicate exercise. It requires application of a "time-marching" explicit solution scheme. Such a scheme is implemented in the dynamic finite difference calculation code FLAC3D. This code also uses mixed-discretization zoning technique which is believed to ensure accurate modeling of plastic collapse loads and plastic flow [*Marti and Cundall*, 1982]. Therefore FLAC3D has been chosen for the numerical tests presented below.

4.1. Setup of Numerical Models

[40] A square 2-D model has properties corresponding to the above constitutive formulation with a constant hardening modulus. The model is uniformly pre-stressed close to

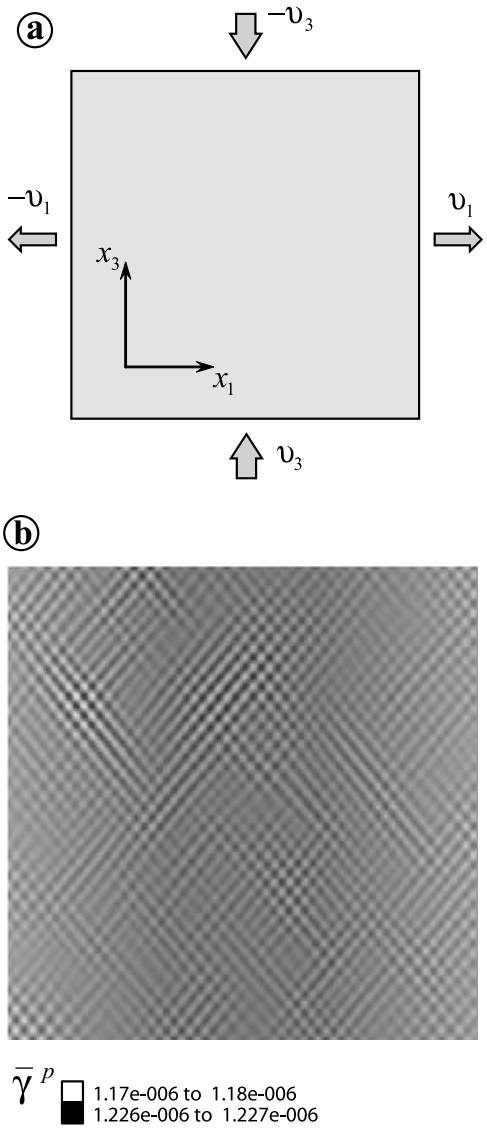

Figure 6. (a) Set up of 2-D numerical models and (b) accumulated inelastic deformation $\bar{\gamma}^p$ pattern at the onset of bifurcation when the whole model is in elasto-plastic state. Constitutive parameters $\alpha = 0.5$, $\beta = 0$, $\nu = 0.3$, $N = 0.21$, and $h = -0.2$ do not change during deformation. The model is initially pre-stressed close to the yield surface and then subjected to the slow velocity boundary conditions: $\upsilon_1 = \upsilon_3 = 10^{-3}$ m/s such that N value remained practically constant during deformation. The model size is 7×7 cm (200×200 numerical grid elements).

the yield surface and then subjected to the velocity boundary conditions (Figure 6a) at plane-strain state. The only difference between the numerical runs is the h value.

4.2. Results

[41] After some elastic straining the yield surface has been reached and initially homogeneous inelastic deformation started. The deformation bifurcation always begins in the continuing loading regime and results in formation of a regular penetrative network of conjugated bands with accelerated and decelerated inelastic deformation (Figure 6b). At the next stage the response of the material outside the bands with accelerated deformation becomes elastic (elastic unloading). The size of the elastic zones rapidly grows and the distance between the "active" localization bands correspondingly increases to a certain value depending on h.

[42] The maximal h at which the deformation bifurcation was clearly observed is about $h \approx -0.08$. The bifurcation started after $\bar{\gamma}^p$ attained a value of $\bar{\gamma}^p_{ld} = 2 \times 10^{-6}$. The deformation pattern during elastic unloading stage reached a stationary state when $\bar{\gamma}^p$ attained a value of about $\bar{\gamma}^p_{unld} = 1.2 \times 10^{-3}$ (the simulation continued to $\bar{\gamma}^p = 3 \times 10^{-2}$). Other models in Figure 7 with smaller h have been run until the same deformation $\bar{\gamma}^p = \bar{\gamma}^p_{unld}$. In all cases the scenario was the same, but for smaller h the bifurcation started at smaller $\bar{\gamma}^p_{ld}$ and resulted in a denser band network. Continuation of deformation over $\bar{\gamma}^p_{unld}$ resulted mainly in propagating the existing bands and did not modify much the average band spacing (Figure 8).

5. Discussion

[43] The spacing parameter χ obtained in the above numerical models strongly depends on the hardening modulus h in accordance with the theoretical prediction (Figure 9). The maximal h value, $h_{\max}$, at which the bifurcation occurs in the numerical trials clearly depends on, and increases with the mesh resolution toward an asymptotic value. In our simulations $h_{\max} \approx -0.08$. This value can be probably further reduced to approach the predicted value $h_{cr} = -0.04$ by refining the model, but this was not our objective. On the other hand, in unloading regime, $h_{\max}$ can never reach h_{cr} even theoretically since in this case the distance between the bands should be infinite.

[44] The minimal h value at which a regular deformation pattern has been obtained in numerical models is near $h = -0.6$, with the corresponding spacing parameter $\chi = 0.6$. The theoretical curve in Figure 9 goes to $\chi = 1$ for which $h_{\min} = -0.86$ and the band thickness d is equal to the inter-band distance λ.

[45] It is seen in Figure 7 that d increases when h grows from $h_{\min}$ to $h_{\max}$. The band segments' length increases with h as well. Since the constitutive formulation being used involves no inherent length scale, d does not represent an actual thickness of the localization band in a real material (even if it has exactly the same properties as the numerical model). The absolute value of d in numerical models is directly related to the grid element size Δl_m and is equal to $q_m \Delta l_m$ where q_m depends on h and practically does not depend on Δl_m. In Figures 7a, 7b, 7c, and 7d, q_m is equal to ca. 6, 4, 3.3, and 3, respectively. In reality d is equal to q_r (a few to several) grain sizes Δl_r as follows from numerous experimental studies (some references can be found for example in [*Bésuelle and Rudnicki*, 2004]). Curiously, both q_m and q_r vary approximately within the same range and it looks like $q_m \approx q_r$. In other words, the band thickness in a numerical model seems to approximately scale with the band thickness in reality, with the scaling factor being $\Delta l_r / \Delta l_m$.

[46] The absolute value of d in the numerical models thus does not have real physical meaning, only the relative thickness does. Relative, for example, to the inter-band distance λ: d/λ (this ratio is equal to the spacing parameter

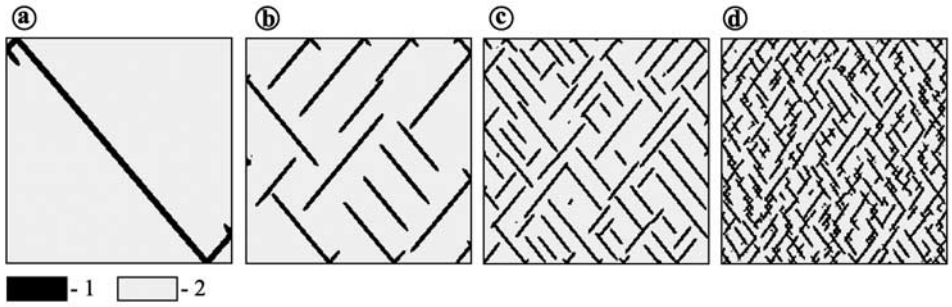

Figure 7. Distribution of loading bands and unloading zones for different h at $\bar{\gamma}^p = 1.2 \times 10^{-3}$. (a) h = − 0.1, $\chi = 0.05$; (b) h = −0.2, $\chi = 0.2$; (c) h = −0.35, $\chi = 0.23$; (d) h = − 0.5, $\chi = 0.42$. The other parameters are the same for all models and specified in the caption to Figure 6. 1, Elasto-plastic state; 2, elastic state. (The spacing parameter χ has been calculated automatically as a ratio of the total area with elasto-plasic state to the total area with elastic state).

χ used in the above theoretical analysis) or to the band length. Reduction of d with h reduction in numerical models (Figure 7) also has a real physical significance, meaning that the closer the h value is to h_{min}, the thinner the band is, not only in the numerical models, but also in reality. In the latter case at sufficiently small h a localization band will appear as a fracture (a shear fracture).

[47] It follows that if h reduces progressively during the loading of a real material, d will reduce as well. If h can be reduced to a sufficiently small value (if the material is sufficiently brittle) then the localization band will become a narrow zone (fracture) located within the band of a damaged material. In other words, the thickness of the active part of the initially wide band will reduce with deformation as long as h reduces.

6. Conclusions

[48] Extending shear-band bifurcation analysis from one band in an infinite body (Figure 2) to band network in a finite body (Figure 3a) along with the results of numerical simulations suggests the following description of this process in a brittle material. The bifurcation starts at normalized hardening modulus $h = h_{max}$, where h_{max} was proven to be the same as that obtained previously from mono-band analysis. The deformation pattern is represented at this stage by two conjugated sets of parallel bands of accelerated and decelerated inelastic deformation. This pattern affects the whole body, is penetrative, and as follows from the theoretical analysis, is not characterized by any specific spacing. On the other hand, numerical models show that at this stage the band thickness is close to the inter-band distance (Figure 6b). At the next stage of bifurcation the response of material outside the localization (loading) bands becomes elastic (elastic unloading). Therefore there is no longer accumulation of inelastic deformation and hence of damage outside the loading bands. On the contrary, the inelastic deformation within these bands is accelerated resulting in increasing damage and hence texture contrast of the material within and outside the bands. This is due to the texture contrast that the bands (incipient fractures) can become distinctive in real conditions in Figure 1. The distance between the bands (spacing λ) rapidly increases (i.e., the area of elastically deforming/unloading zones becomes larger). This distance is very sensitive to h such that $\lambda = \infty$ at $h = h_{max}$ and λ tends to zero (to the band thickness)

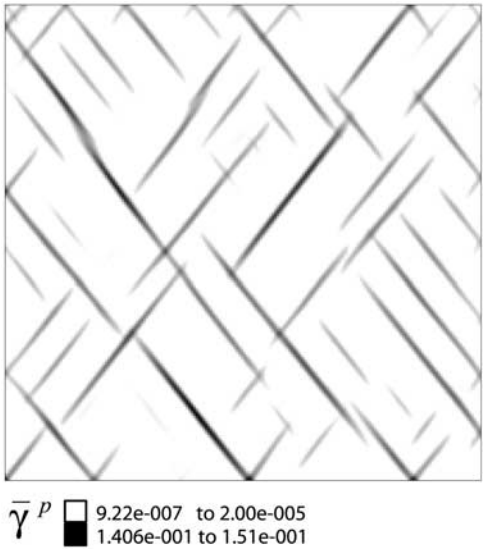

Figure 8. $\bar{\gamma}^p$ pattern in the model in Figure 7c run to larger deformation $\bar{\gamma}^p = 0.15$.

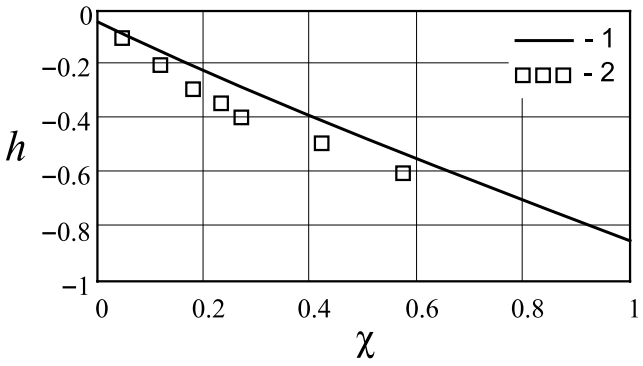

Figure 9. Relation between the spacing parameter χ and the hardening modulus h: comparison of theoretical and numerical results for $\alpha = 0.5$, $\beta = 0$, $\nu = 0.3$, and $N = 0.21$. 1, Theoretical curve; 2, points obtained from the numerical models.

when h is reduced to a certain minimal value h_{min} depending on the constitutive parameters and the stress-state (Figure 5). If h is always larger than h_{max}, the bifurcation does not occur at all. If h is reduced rapidly below h_{min}, the deformation "jumps" into the post-localization state and the material becomes completely crushed as is observed, for example, during deformation of glass. The λ value depends also on the stress-state and is generally smaller for smaller Lode-type parameter $|N|$ and larger for the stress-state approaching the axi-symmetric loading when $|N| \rightarrow \sqrt{1/3}$. The obtained solution shows how λ depends on other parameters as well. For example, in the case of axi-symmetric compression and negative dilation factor β, λ decreases with an increase in the internal friction α (at $h = const$), while for positive β this tendency reserves. For $\alpha = 0.5$, λ rapidly increases with increase in β (Figure 4).

[49] Although the above results were obtained within the frame of bifurcation analysis dealing only with the onset of constitutive instability, the numerical models show that the above conclusions remain valid for larger deformation (compare, for example, Figures 7c and 8). These results can be used for estimating the spacing λ of the fracture network from the material properties and the information about the stress-state. Of course such estimation will be very approximate and will reflect only "genuine" or primitive fracturing which is not affected by the heterogeneities in the material properties and boundary conditions. The boundary effects are especially important in the rock mechanics experiments. According to the reported results, the localization/fracturing (the second stage of bifurcation with interband unloading) within the rock sample should start at the hardening modulus small enough ($h < h_{max}$) for the spacing λ to be smaller than the sample size. The sample failure should follow this stage. However, in reality the deformation may localize well before this because of the stress concentration caused by the boundary effects due in particular to non-zero friction along the sample boundaries.

[50] Finally, the knowledge of solution $\chi(\alpha, \beta, \nu, N, h)$ and in particular of two critical hardening moduli h_{max} and h_{min} is important when setting up the numerical models of a process that involves a constitutive instability. Without this knowledge and the corresponding adjustment of the mesh resolution, boundary conditions, and dynamic dumping parameters, the instability may be not "caught" by the model.

[51] **Acknowledgments.** The author is grateful to I. Garagash for many helpful discussions on the bifurcation theory, and to two reviewers for the constructive review.

References

Berg, C. A. (1970), Plastic dilatation and void interaction, in *Inelastic Behaviour of solids*, edited by M. F. Kanninen et al., pp. 171–209, McGraw-Hill.

Bésuelle, P., and J. W. Rudnicki (2004), Localization: Shear Bands and Compaction bands, in *Mechanics of Fluid-Saturated Rocks*, edited by Y. Guéguen. and M. Boutéca. pp. 219–321, Academic Press.

Garagash, I. A. (1981), On the internal instability of materials with damage plasticity, *Proc. Kazach. Acad. Sci.*, (3), 2–7, (in Russian).

Garagash, I. A., and V. N. Nikolaevsky (1989), Nonassociated flow rules and localization of plastic deformation, in *Advances in Mechanics*, vol. 12, No 1, pp.131–183, Warzawa (in Russian).

Hadamard, J. (1903), *Leçons sur la propagation des ondes et les équations de l'hydrodynamique*, A. Hermann, Paris.

Hill, R. (1962), Acceleration waves in solids, *J. Mech. Phys. Solids*, *10*, 1–16.

Issen, K. A., and J. W. Rudnicki (2000), Conditions for compaction bands in porous rocks, *J. Geophys. Res.*, *105*, 21,529–21,536.

Mandel, J. (1964), Propagation des surfaces de discontinuité dans un milieu élastoplastique, in *Stress waves in anelastic solids*, pp.331–341, Springer-Verlag, Berlin.

Mandel, J. (1966), Conditions de stabilité et postulat de Drucker, in *Rheology and soil mechanics*, edited by J. Kratchenko and P. M. Sirieys, pp. 58–68, Springer-Verlag, New York.

Marti, J., and P. A. Cundall (1982), Mixed discretization procedure for accurate solution of plasticity problems, *Int. J. Num. Methods Anal. Methods Geomech.*, *6*, 129–139.

Nadai, A. (1950), *Theory of flow and fracture of solids*, vol. 1, 2nd edn., McGraw-Hill, New York.

Nikolaevskiy, V. N. (1967), On the relation between shear and volumetric plastic deformation and shock waves in soft soils, *Proc. USSR Acad. Sci.*, *177*(3), 542–545, (in Russian).

Perrin, G., and J. B. Leblond (1993), Rudnicki and Rice's analysis of strain localization revisited, *J. Appl. Mech.*, *60*, 842–846.

Poliakov, A. N., H. J. Herrmann, Yu. Yu. Podladchikov, and S. Roux (1994), Fractal plastic shear bands, *Fractals*, *2*(4), 567–581.

Reynolds, O. (1885), On the dilatancy of media composed of rigid particles in contact. With experimental illustrations, *Phil. Mag.*, *20*(127), 469–481, S.5.

Rice, J. R. (1973), The Initiation and Growth of Shear Bands, in *Plasticity and Soil Mechanics*, edited by A. C. Palmer, pp. 263–274, Cambridge Univ. Engineering Department, Cambridge.

Rice, J. R. (1976), The localization of plastic deformation, in *Theoretical and Applied Mechanics* (Proceedings of the 14th International Congress on Theoretical and Applied Mechanics, Delft), edited by W. T. Koiter Vol. 1, pp. 207–220, North-Holland Publishing Co.

Rice, J. R., and J. W. Rudnicki (1980), A note on some features of the theory of localization of deformation, *Int. J. Solids Struct.*, *16*, 597–605.

Rudnicki, J. W., and J. R. Rice (1975), Conditions for the localization of deformation in pressure-sensitive dilatant materials, *J. Mech. Phys. Solids*, *23*, 371–394.

Thomas, T. (1961), *Plastic Flow and Fracture in Solids*, Academic press, New York, 267pp.

Vardoulakis, I., and J. Sulem (1995), *Bifurcation analysis in geomechanics*, Blackie Academic and Professional, pp. 462, New York.

Wibberley, C. A. J., J-.P. Petit, and T. Rives (2007), The mechanics of fault distribution and localization in high-porosity sands, Provence, France, in *The Relationship between Damage and Localization*, edited by H. Lewis, and G. D. Couples, Geological Society, London, Special Publications, 289, 19–46.

A. I. Chemenda, Géosciences Azur, Université de Nice-Sophia Antipolis and CNRS, 250 Rue Albert Einstein, 06560 Valbonne, France. (chemenda@geoazur.unice.fr)